

Optical strain measurements and its finite element analysis of cold workability limits of pure aluminium

J. Babu Rao^{1*}, Syed Kamaluddin² and N.R.M.R. Bhargava³

^{1,3} Dept of Metallurgical Engineering, Andhra University College of Engineering, Visakhapatnam – 530 003, INDIA

² Dept of Mechanical Engineering, GITAM College of Engineering, Visakhapatnam – 530 045, INDIA

*Corresponding Author: e-mail: baburaojinugu@yahoo.com

Abstract

In the present research work a new method of optical strain measurement (Machine vision system) was proposed for the analysis of flow behaviour of pure aluminium as a function of friction, aspect ratio and specimen geometry. Implementation of this new method reduced the extent of experimentation. Eight standard shapes of the axisymmetric specimens of cylindrical with aspect ratios 1.0 and 1.5, ring, flanged and tapered were selected for the present investigation. Specimens were deformed in compression between two flat platens to predict the metal flow at room temperature. A 4 X 4 mm square grid was marked at mid plane of the standard specimens. Online video images of square grid were recorded during the deformation process till the crack initiation. The distortions of grid from recorded images were analyzed offline. Finite element software ANSYS has been applied for the analysis of the upset forming process. The FEA results were compared with the analytical results of various stresses from the experimental measurements of axial, circumferential strains and found to be in good agreement. Ring compression tests with its finite element analysis were carried out to determine the friction factor (m) between the die and work piece and same found to be 0.3.

Keywords: Friction, Upsetting, Machine vision system, Finite Element Analysis

1. Introduction

During metal forming, effective ductility depends on localized conditions of stress, strain, strain rate and temperature in combination with material characteristics such as impurity content and grain size, processing parameters associated with die design, work piece geometry and lubrication. Several investigators used compression test on cylindrical specimens for the study of deformation behavior under combined stresses (Kudo *et al.*, 1967; Thomason, 1969; Kobayashi, 1970; Kuhn *et al.*, 1971). The demand for more efficient manufacturing processes has been increasing in the last few decades. Computer simulation has become reliable and acceptable in the metal forming industry. Finite Element Analysis (FEA) is widely used in metal forming analysis due to its capability to model the complicated geometries of tools and parts in forming process (Jolgaf *et al.*; Rajiv, 2004; Altan *et al.*, 2002; Vazquez *et al.*, 2000; Kobayashi *et al.*, 1989). Considerable efforts have been made largely in a research environment, to apply FEA to the simulation of forging operations and in evaluating the results. FE codes, which will analyze the plastic deformation of metals, are available but are often not readily useable by non-experts.

During compression of a cylinder the lateral free surface barrels and results in the development of a tensile stress in the circumferential direction. Severe barreling causes the axial stress to become tensile. Proper control on cylinder height-to-diameter ratio and the friction at the contact surfaces can maximize barrel curvature. Work-die interface friction is of great importance in any metal forming operation. It affects the detailed material flow and the deformation characteristics of the work piece, the wear and fatigue failure of the tool, and the mechanical properties of the formed parts. Good surface finish or low frictional constraint is always the key to a viable cold working process. Knowledge of material behavior requires the measurement of mechanical parameters. The non-contact and non-destructive methods can represent a real advance for displacement, stress and strain measurements. Control of these parameters may thus be exercised to produce conditions favorable for enhanced deformation to

fracture. Present investigation attempts to study the deformation behavior of Aluminium by upsetting at room temperature using Machine vision system. Aspect ratio, specimen geometry and friction at contact surfaces were studied as process parameters. Machine vision system has been adopted to study and analyze the flow behavior of materials during upsetting, which minimizes experimentation process.

2. Experimental Procedure

Commercial pure aluminum (EC grade, 99.5 + % pure) ingot, procured from Hindalco was cast into 170 X 18 Φ mm, cylindrical fingers. Standard samples (shown in figure 1) of cylindrical with aspect (H_0 / D_0) ratios of 1.0, 1.5., ring, flanged and tapered specimens of standard dimensions were prepared using conventional machining operations of turning, facing, drilling and boring. Sample geometry and specifications were given in tables 1& 2. The average surface roughness at the flat and curved surfaces of the specimens was measured as 4 microns and 3 microns respectively. Surf tester was used for the measurement.

Ring compression tests were conducted to determine the friction factor ‘m’ for a given set of flat platens. Standard ring compression samples were prepared with the ratio of Out side Diameter: Inside Diameter: Height = 6: 3: 2 (48: 24:16 mm). The deformation was given slowly with a ram speed of 0.25 mm/sec using Fuel Instruments & Engineers Pvt. Ltd (FIE) India make Compression Testing Machine (Model: CTM -1M30-0113, 200T capacity). One set of cold work die steel dies (flat platens) were machined in varying conditions of machining to produce smooth finish (4 microns surface roughness to yield low friction). Standard samples were upset by placing between the flat platens at a constant cross head speed of 0.5 mm/min for given friction condition, using a computer controlled servo hydraulic (Model: FIE-UTE-100T) universal testing machine, as shown in Figure 2.

Table 1: Specimen sample shapes and dimensions, all the dimensions are in mm.

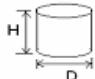
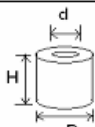

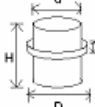
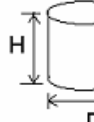
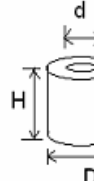
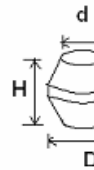

Geometrical shape	H_0/D_0	H	D	d	t
	Solid cylinder (H_0/D_0) = 1.0	20	20	---	---
	Ring (H_0/D_0) = 1.0	20	20	10	---
	Taper (H_0/D_0) = 1.0	20	20	10	5
	Flange (H_0/D_0) = 1.0	20	25	10	5

Table 2: Specimen sample shapes and dimensions, all the dimensions are in mm.

Geometrical shape	H_0/D_0	H	D	d	t
	Solid cylinder (H_0/D_0) = 1.5	30	20	---	---
	Ring (H_0/D_0) = 1.5	30	20	10	---
	Taper (H_0/D_0) = 1.5	30	20	10	5
	Flange (H_0/D_0) = 1.5	30	25	10	5

A PC based system consisting of a video camera with an integrated digitizing capacity, 640 X 480 pixels resolution, 256 colour, full depth, 20 pictures per second shutter speed, mounted with a magnifying lens was used to record the images of the upsetting process. A 4 X 4 mm square grid was marked at mid height of the standard specimens. Online video images of grid were recorded during the deformation process till the crack initiation. The distortions of grid from recorded images were analyzed offline. The images were selected at deformation steps of 5% using the software animation shop 3.0 and were transported to paint shop pro 7.0 for further processing to get the enhanced noiseless images of high clarity grid.

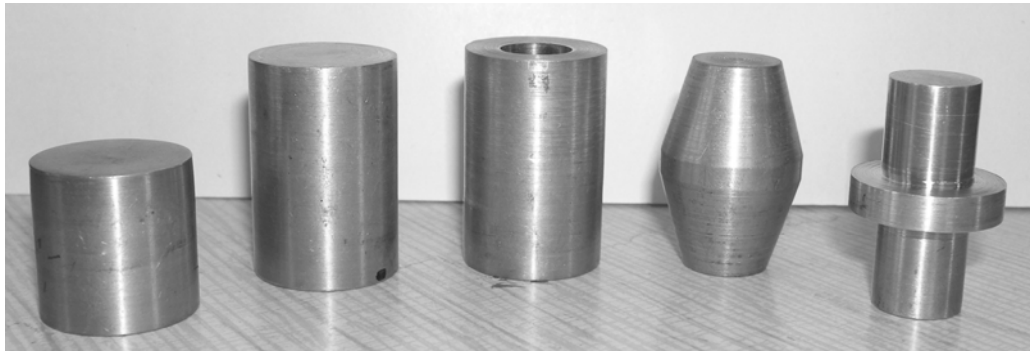


Figure 1: Photograph showing the cylindrical samples for upsetting, with different geometries of H_0/D_0 ratio. (a) 1.5 (b) 1.0 and Ring, Tapered and Flanged

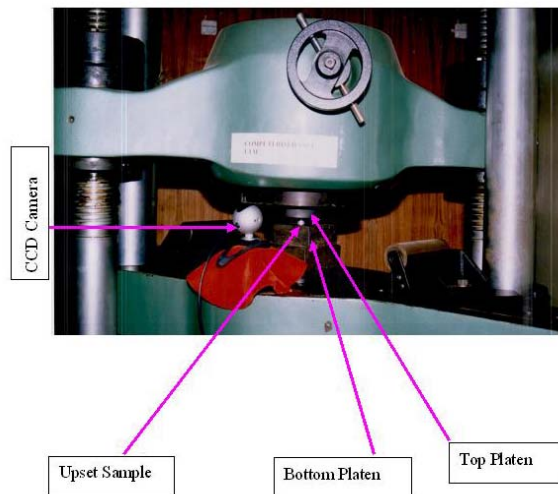


Figure 2: Experimental set up of pc based on line video recording system for grid measurement during upsetting on 100T computer controlled servo hydraulic UTM

The axial and the circumferential (hoop) strains are calculated for each element from the measurements obtained according to:

$$\epsilon_z = \ln \left(\frac{h_i}{h_0} \right) \quad \text{and} \quad \epsilon_\theta = \ln \left(\frac{w_i}{w_0} \right)$$

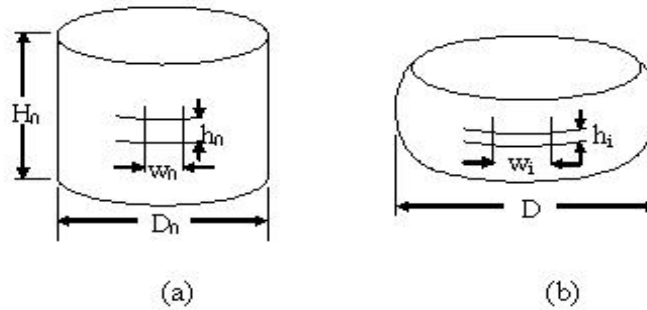


Figure 3: Schematic diagram of upset tests showing grids for strain measurements

Where: h_0 and w_0 are the initial height and width of an element (figure 3a) respectively, and h_i and w_i are the current height and width of the element respectively (figure 3b).

3. Results and Discussion

3.1 Friction factor determination

The decrease in internal diameter of the ring compression test was plotted against the deformation on Male and Cockcroft (Male et al., 1964) calibration curves in increments of 10% deformation, as shown in Figure 4 (a). When these ring compression values were fit into calibration curves for the given set of dies, it was found that the friction factor ‘m’ with high finish dies was nearly equal to 0.30. The same set of dies was used for upset tests. Figure 4 (b) shows the ring compression specimen of before and after deformation.

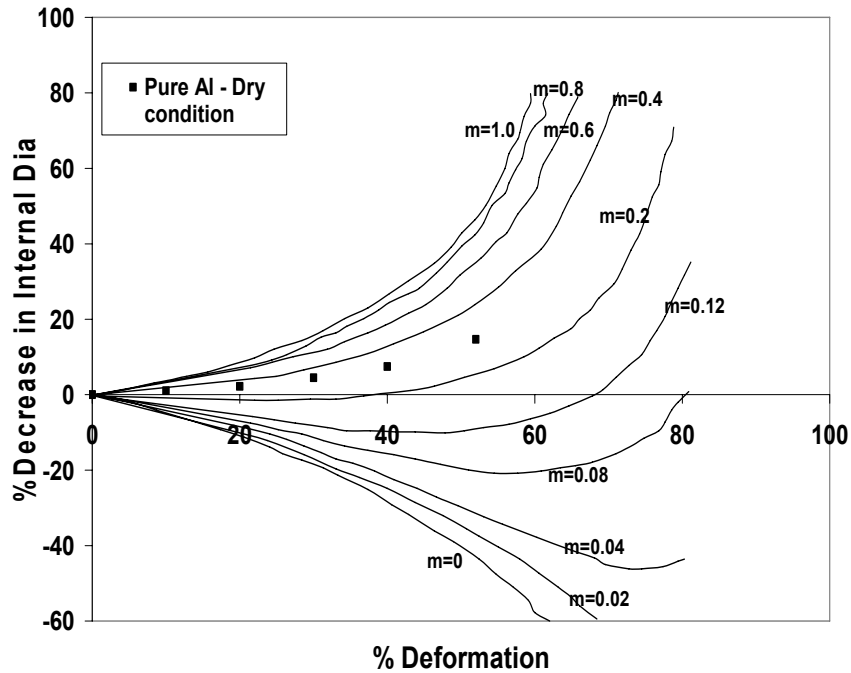


Figure 4 (a): Ring test calibration curves. Changes of the minimum internal diameter as a function of the reduction in height for Dry condition

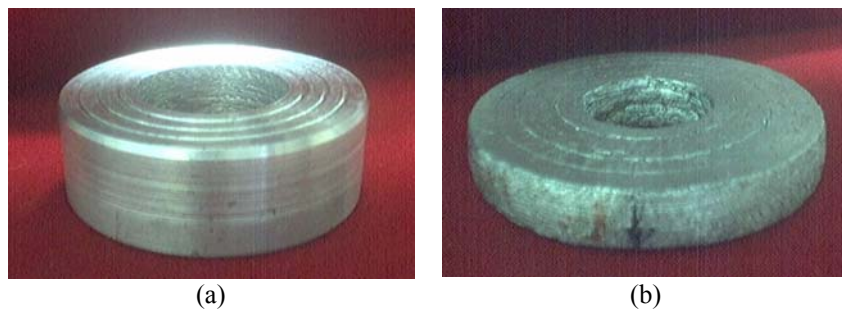


Figure 4 (b): Ring compression specimen (OD: ID: H = 6:3:2) (a) Undeformed (b) 50% deformed under dry condition (friction factor ‘m’=0.3).

3.2 Finite Element Analysis of Ring Compression Test

Finite element analysis of ring compression test was carried out at friction factor (m) = 0.30. Rigid-flexible contact analysis was performed for this process. For such analysis, rigid tools need not be meshed. The ring specimen was meshed with 10-node tetrahedral elements (solid 92 in ANSYS Library). Element size was selected on the basis of convergence criteria and computational time. The program will continue to perform equilibrium iterations until the convergence criteria are satisfied. The results of the FE analysis for ring compression shows that decrease in the average inside diameter against deformation has a variation of about 10% compared to experimental results. Figure 5 shows undeformed mesh and deformed mesh after 50% deformation of the FEA models of ring compression test (OD:ID:H = 6:3:2) with m=0.30.

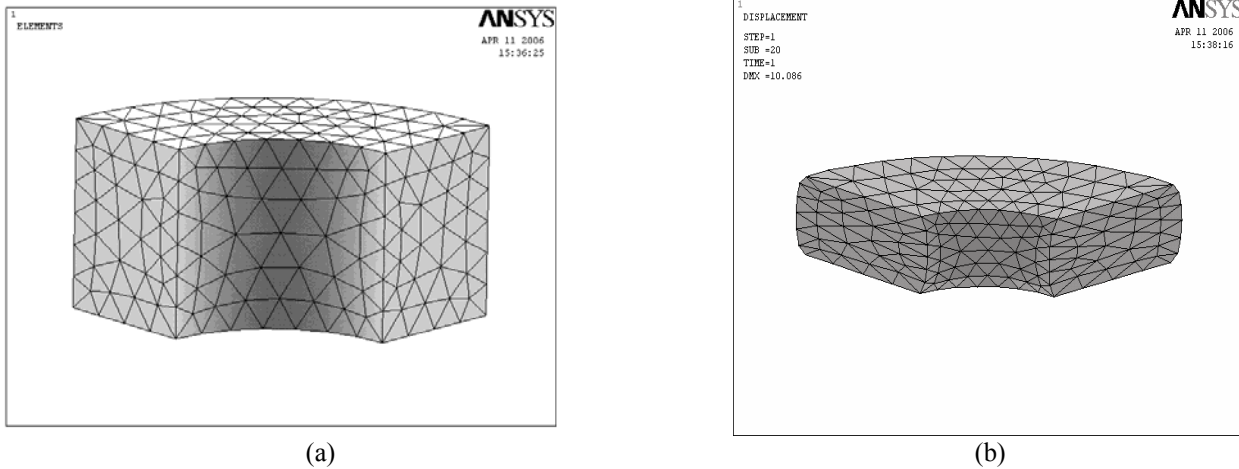


Figure 5: Quarter FEA model of ring specimen (a) Undeformed (b) 50% Deformed

3.3 Flow curves

Load - displacement curves were shown in figure 6 for Aluminium under given friction conditions for all the geometry of the components. From these curves, all the shapes of the Aluminium specimens were observed to be taking more loads while increasing the deformation. Further an increase in aspect ratio decreases the load required for the same amount of deformation. For a fixed diameter, a shorter specimen will require a greater axial force to produce the same percentage of reduction in height, because of the relatively larger undeformed region (Dieter, 1928). Present experimental results were in significance with the above discussion. As per the geometry of the specimen is concerned, to deform the component, tapered specimen required more load than ring and flanged specimens. The experimental loads reveal that geometry of the object also effect the load required for the deformation process.

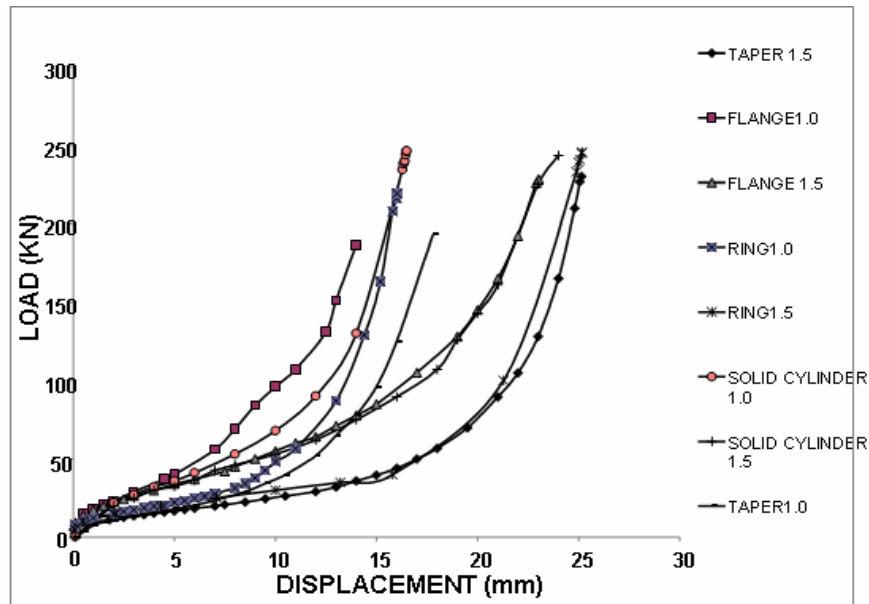


Figure 6: Load – displacement curves for Aluminium at friction factor ‘m’=0.30.

The true stress-true strain curve was obtained from the frictionless, slow speed compression test at room temperature of cylindrical specimen with height to diameter ratios, $H_0/D_0 = 1.0$ and fit into well established Hollomon power law (Gouveia et al., 1996; Ungár et al., 2001; Iwahashi et al., 1998; Komura et al., 1999; Parteder et al., 1998; Hollomon, 1945; Tong, 1998; Johs, 1969) given by

$$\bar{\sigma} = K \bar{\epsilon}^n = 136 \bar{\epsilon}^{0.19} \text{ (MPa)}$$

Where: $\bar{\sigma}$ = True stress, $\bar{\epsilon}$ = True plastic strain, K = Strength coefficient, and n = Strain hardening exponent.

This data was used as input for finite element simulation and analysis of upsetting process. The specimens of various geometries of Aluminium which were subjected plastic deformation by upsetting up to the fracture initiation. During upsetting process it was

observed that the five basic geometries of the Aluminium components did not show any initiation of crack up to 60% of deformation under specified frictional condition. Due to practical difficulties in observing the crack initiation, the maximum deformation is limited up to 60% only. Aluminium samples deformed to 60% for friction factor ' m '=0.30 is shown in figure 7. It was observed that decrease in aspect ratio increased the barreling.

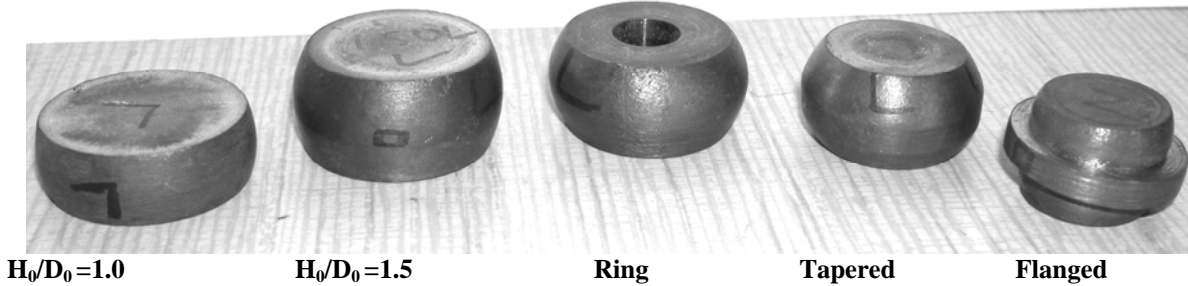


Figure 7: Aluminium samples deformed to 60% for friction factor ' m '=0.30

3.4. Experimental Strain and Stress analysis using Machine vision system

Surface strains, (ϵ_θ) and (ϵ_z) were evaluated for the geometric mid-sectional grid of the specimens (Figure 8) and the results were plotted in figure 9. Upset tests with friction produce curved strain paths. Some of these equations for eight strain paths obtained from different specimens are given in Appendix A. The ends of the strain paths represent the fracture or maximum deformation points. Joining of all these points of all strain paths gives the workability limit for the alloy considered. The deviation of slope of the experimentally determined relationship between axial strain ϵ_z and circumferential strain (hoop strain) ϵ_θ , from that corresponding to homogeneous deformation represents barreling. This deviation was less when the specimen - die interface friction was low. The strain paths for $H_0/D_0=1.0$ are much steeper than $H_0/D_0=1.5$ in specified friction conditions. For ring specimen the flow of the material was dominant on the outer periphery compared to the inside periphery of the mid section. The deviation from homogeneous deformation was observed to be more for the flange specimen than the other specimens for the aspect ratios of 1.0 and 1.5. Flanged and tapered specimen geometries may be regarded as specimens artificially prebulged by machining (Erman, 1983; Gouveia, 1996). Flanged specimens exhibit a strain path similar to that found in axial tension tests, because little or no axial compression was applied to the rim during the circumferential expansion caused by the deformation. Tapered specimens undergo strain evolution somewhere between tension and compression tests.

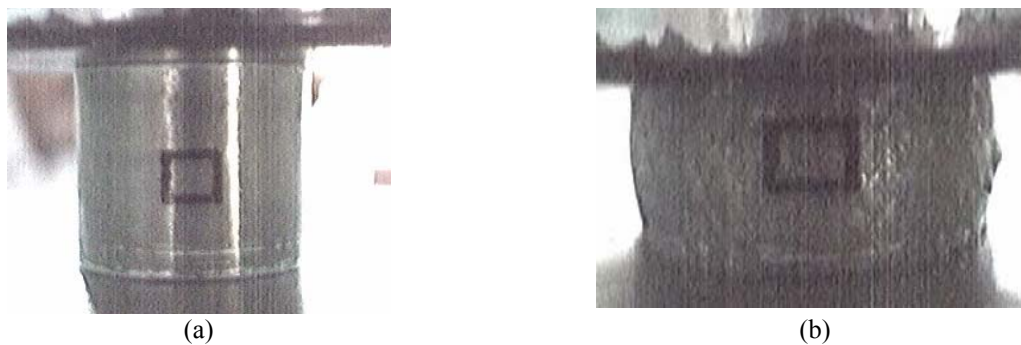


Figure 8: Schematic diagram of upset test showing grids for strain measurements. (a) Images of grids drawn at equatorial plane before deformation (b) after deformation.

The knowledge of the experimental plastic strain history allows the experimental evaluation of stress components with the undergoing deformation (Rao et al., 2009). Effective stress ($\bar{\sigma}$), and stress components σ_θ , σ_z and σ_H as a function of effective strain ($\bar{\epsilon}$) calculated from grid measurements of images obtained from vision technique for Aluminium under specified friction condition for aspect ratios of 1.0 and 1.5 of solid cylinder, tapered, ring and flanged were represented in Figure 9. In an idealized situation of uniaxial compression, the hoop stress σ_θ , is zero and the axial stress (σ_z) is equal to the yield stress (σ_0). Under this condition the hydrostatic component of the stress (σ_H) would be equal to $\sigma_z/3$ and would always be compressive; a state of instability will never occur in homogeneous deformation. Hence according to an instability theory of fracture ductile fracture will never occur in homogenous deformation. On the other hand if the friction between the specimen and platens is such that the deformation departed from the homogeneous case, barrel is developed. The tensile circumferential surface stress component (σ_θ) is non zero and the hydrostatic component of stress (σ_H) become less compressive and in some cases tensile.

The present results, referring to Figure 10, shows that with the increasing friction constraint, the hoop stress component (σ_θ) increasingly becomes tensile with continued deformation. The increase in its value was found to be more in case of specimens deformed under low aspect ratio compared to the high aspect ratios. On the other hand the axial stress (σ_z) increased in the very initial stages of deformation but started becoming less compressive immediately as barreling developed. For unfractured specimens the axial stress (σ_z) will always be compressive. However for the specimens where surface fracture occurred both σ_z and σ_H stress components became less and less compressive as deformation progresses and become tensile. The hydrostatic stress involves only pure tension or compression and yield stress is independent of it. But fracture strain is strongly influenced by hydrostatic stress (Dieter, 1988; Brozzo, *et al.*, 1972). Increase in friction constraint and decrease in aspect ratio caused hydrostatic stress to be tensile and instability starts. As the hydrostatic stress becomes more and more tensile, a state of tensile instability will occur. The transformation in nature of the hydrostatic stress from compressive to tensile depends on the shape and size of the specimen and the frictional constraint at the contact surface of the specimen with the die block.

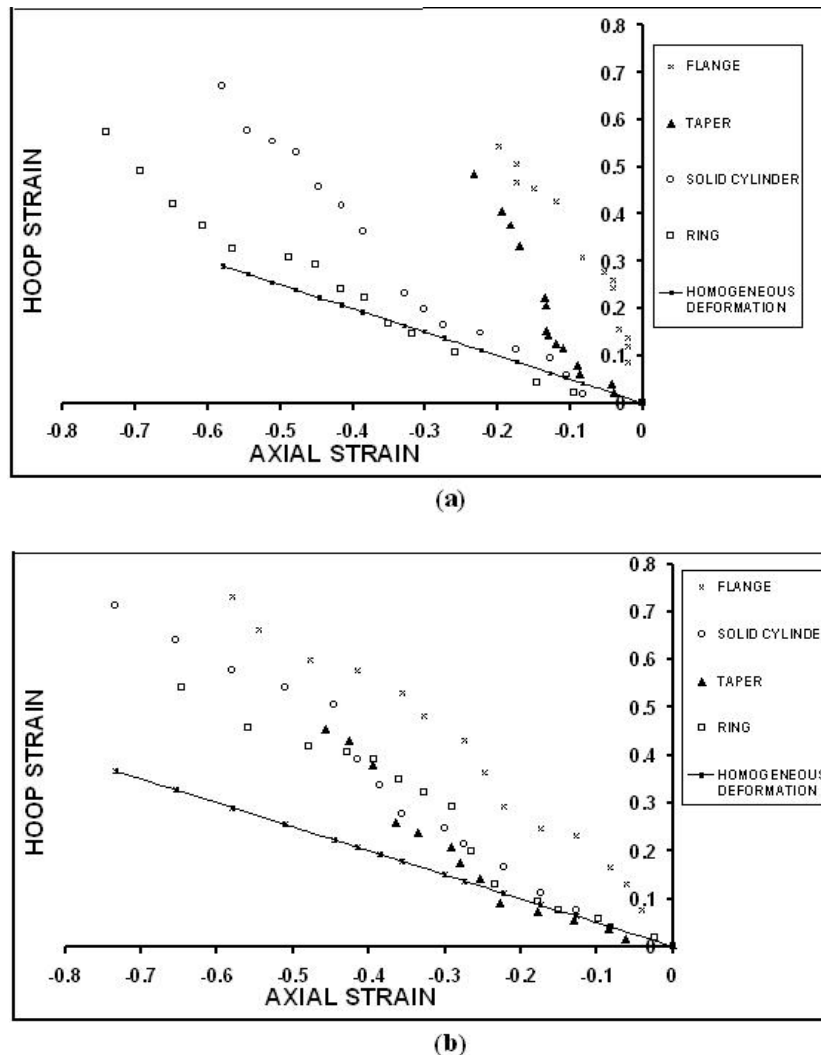


Figure 9: Circumferential (Hoop) strain ϵ_θ as a function of axial strain ϵ_z at the equatorial free surface for Aluminium (with friction factor 'm' = 0.30) (a) $H_0/D_0 = 1.0$ (b) $H_0/D_0 = 1.5$.

From the observation of Figure 10, showing hydrostatic stress as a function of effective strain, it was concluded that for the same amount of strain hydrostatic stress changes quickly from compressive to tensile for small aspect ratios. The nature of hydrostatic stress on the rim of the flanged specimen was tensile from the beginning of the deformation while the axial stress on the rim was almost zero and the circumferential stress coincides with the effective stress of the material. The nature of hydrostatic stress for ring, tapered specimens lie between the regions of cylindrical with aspect ratio 1.5 and the flanged specimens. For the Aluminium, the extent of deformation from instability to fracture is large. However this post instability strain to fracture can be increased by changing the microstructure via proper heat treatment.

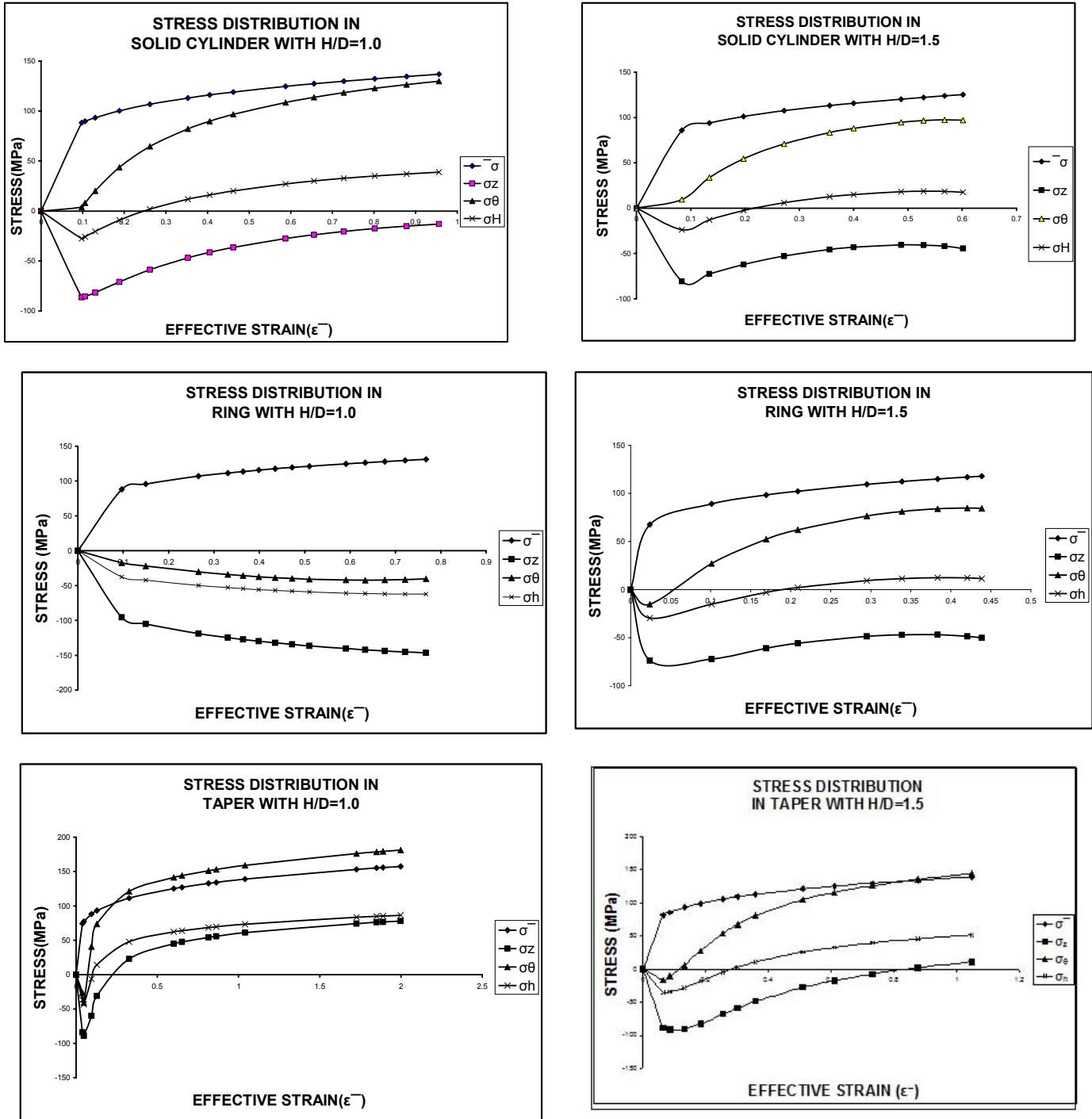


Figure 10: Effective stress ($\bar{\sigma}$), stress components σ_θ , σ_z and σ_H as a function of Effective strain ($\bar{\epsilon}$) for Aluminium under friction factor 'm'=0.30.

3. Finite element modeling

Finite element analysis of deformation behavior of cold upsetting process was carried out with aspect ratios of 1.0 and 1.5 for cylindrical, ring, tapered and flanged specimens. Since computers with high computational speed are now available in the market, the time of computation is not a major constraint for solving the problems of small sized 3-D models. Further, the tetrahedral elements can easily be accommodated in any shape [Wu, et al]. This reduces the number of iterations and steps to be solved. Owing to these facts the present problem is solved using 3-D model. The analysis can also be extended to non axisymmetric problems using a full 3-D model. In the present analysis, quarter portion of 3-D model was considered with symmetric boundary conditions.

Rigid-flexible contact analysis was performed for the forming process. For such analysis, rigid tools need not be meshed. The billet geometry was meshed with 10-node tetrahedral elements (solid 92 in ANSYS Library). Element size was selected on the basis of convergence criteria and computational time. Too coarse a mesh may never converge and too fine a mesh requires long computational time without much improvement in accuracy. The program will continue to perform equilibrium iterations until the convergence criteria are satisfied. It will check for force convergence by comparing the square root of sum of the squares (SRSS) of the force imbalances against the product of the SRSS of the applied loads with a tolerance set to 0.005. Since the tolerance value in the program is set to 0.5%, the solution will converge, only if the out of balance force is very small leading to more accurate results. Material models selected were based on the properties of the tooling and billet materials. Due to high structural rigidity of the tooling, only the following elastic properties of tooling (H13 steel) were assigned assuming the material to be isotropic [<http://www.matweb.com>]. Young's Modulus $E = 220$ GPa and Poisson's ratio $\nu = 0.30$.

For billet material model selected is isotropic Mises plasticity with $E = 110$ GPa, $\nu = 0.343$ and plastic properties obtained from Hollomon power law equation. As the nature of loading is non-cyclic, Bauschinger effect could be neglected and the non-linear data was approximated to piecewise multi linear with 10 data points. Care is taken that the ratio of stress to strain for first point equals to Young's modulus of Aluminium. The material was assumed to follow the Isotropic hardening flow rule. Suitable elastic properties were also assigned for the material chosen for analysis. As the experiments were conducted at room temperature, the material behavior was assumed to be insensitive to rate of deformation (Kobayashi, 1970; Lee *et al.*, 1973; Zeinkiewicz, 1984).

A 3-D, 8-noded, higher-order quadrilateral element CONTA 174 (of ANSYS library) that can be located on the 3-D solid or shell elements with mid side nodes is used. It can be degenerated to 3-7 node quadrilateral/triangular shapes. Contact surface was meshed with CONTA 174. TARGE 170 (of ANSYS library) is used to represent various 3-D target surfaces for the associated contact elements. The contact elements themselves overlay the solid elements describing the boundary of a deformable body that is potentially in contact with the rigid target surface, defined by TARGE 170 [Ansys 8.0 reference manual, 2006]. Hence a target is simply a geometric entity in space that senses and responds when one or more contact elements move into a target segment element.

4. Validation of FEA Results

Figure 11 shows the specimens before deformation. There was zero friction at metal-die contact and no apparent bulging; the deformation can be treated as homogeneous, Figure 12. The variation in the values of radial diameter at 50% deformation obtained from finite element analysis and calculated values from volume constancy condition is 0.7% shown in Table 3. This small variation may be neglected in non linear finite element analysis such as in large deformation / metal forming applications.

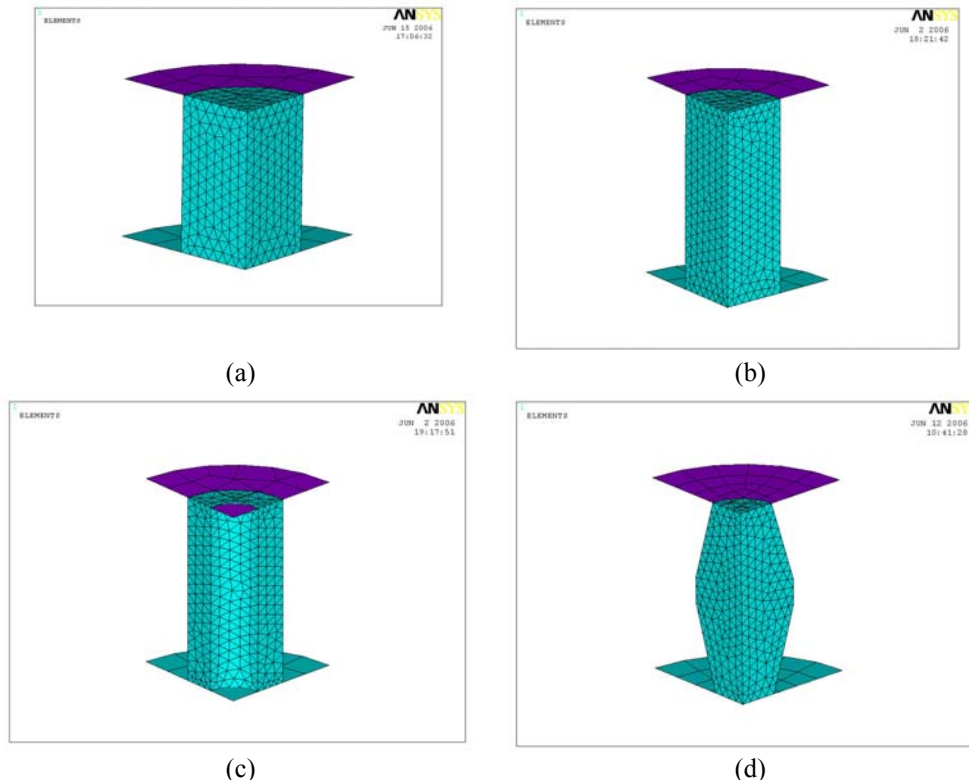
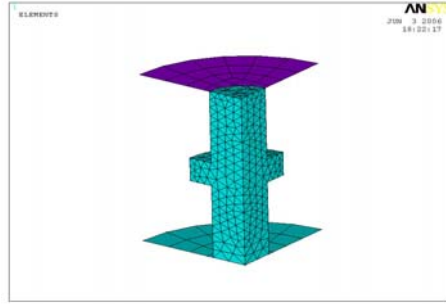


Figure 11: FEA modeled Undeformed specimens (a) Cylindrical specimen, $H_0/D_0 = 1.0$ (b) Cylindrical specimen, $H_0/D_0 = 1.5$ (c) Ring (d) Tapered.



(e)

Figure 11: FEA modeled Undeformed specimens (e) Flanged

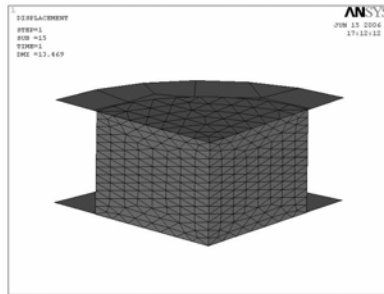


Figure 12: FEA model with $H_0/D_0 = 1.0$ at 50% deformation under zero friction condition

Table 3: Variation between values of radial diameter after 50% deformation at zero friction condition

Diameter obtained from analytical calculations, mm	Measured diameter from FEA, mm	% Variation
$25 \times \sqrt{2} = 35.355$ (Assuming volume constancy)	$25 + 2 \times 5.054 = 35.108$ (Figure 11)	0.7

All the Aluminium specimens were modeled and were analyzed for 50% deformation using ANSYS package. The analysis was performed for all the specimens chosen and the results of sub-grid quantities equivalent to the grid drawn on the sample during the upset test were noted. The increase in barreling was observed with decreasing aspect ratio of 1.0 as shown in figures 12 and 13. Friction hills containing relatively undeformed zones were being observed as conical portions in both the cases, with the apex of cone on the axis.

The hydrostatic stress (σ_H) profiles for Aluminium under given friction conditions, cylinder, ring, flanged and tapered were shown in figures from 13 to 17 at 50% deformation. The stress values were compared for various stress values obtained after 50% deformation from finite element analysis and measurement of grids using Machine vision system. All these results were in close agreement to experimental values with a maximum error of less than 15%.

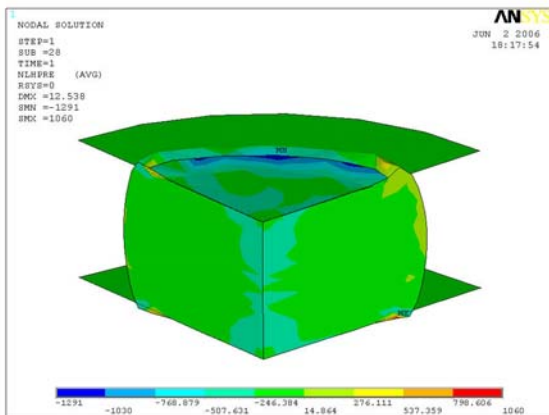


Figure 13. Hydrostatic stress at 50% deformation (Cylinder, $H_0/D_0= 1.0$) of Aluminium under Friction factor ($m=0.30$) condition.

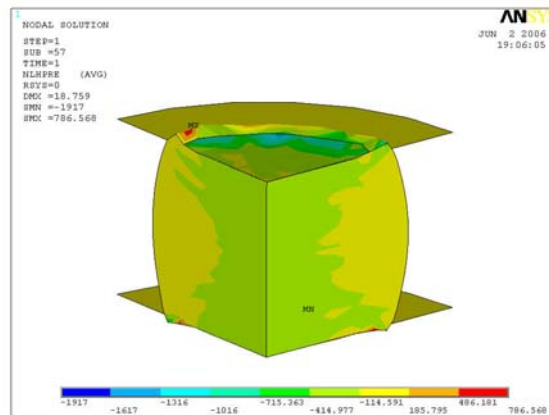


Figure 14. Hydrostatic stress at 50% deformation (Cylinder, $H_0/D_0=1.5$) of Aluminium under friction factor ($m=0.30$) condition.

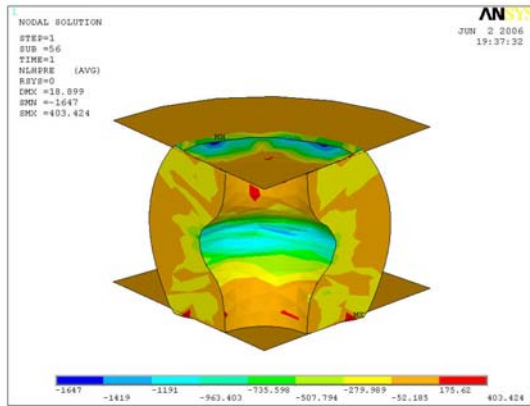


Figure 15: Hydrostatic stress at 50% deformation (Ring) of Aluminium under friction factor ($m=0.30$) condition.

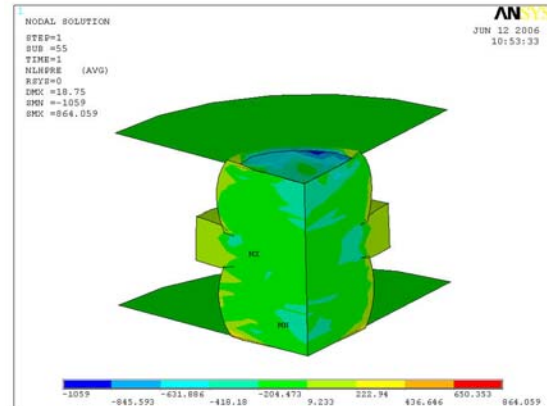


Figure 16: Hydrostatic stress at 50% deformation (Flanged) of Aluminium under friction factor ($m=0.30$) condition.

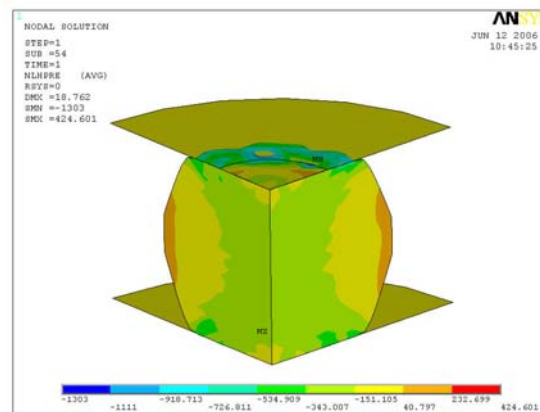


Figure 17: Hydrostatic stress at 50% deformation (Tapered) of Aluminium under friction factor ($m=0.30$) condition.

5. Conclusions

- Inverse FEA modeling and analysis was successfully performed from the experimentally obtained friction factor values.
- Machine vision system was successfully employed in the measurement of grid distortion at equatorial surface for the analysis of stress components. Implementation of Machine vision system reduced the extent of experimentation.
- With decrease in aspect ratio, the circumferential stress component increased monotonically. At the beginning of deformation axial compressive stress increased in magnitude but as the deformation progresses the magnitude reduced. Hydrostatic stress also reduced in magnitude as the deformation increased. Increase in friction constraint and decrease in aspect ratio caused hydrostatic stress to be tensile.
- The nature of hydrostatic stress on the rim of the flanged specimen is found to be tensile.
- The nature of hydrostatic stress for ring, tapered specimens lie between the regions of cylindrical with aspect ratio 1.5 and the flanged specimens.
- Results obtained by finite element analysis closely matched with the experimental values and hence the model is validated.

Acknowledgements

The authors thank the AICTE, New Delhi for their financial support under AICTE – CAYT scheme (File No:1-51/FD/CA/(19) 2006-2007) and also the Departments of Metallurgical and Civil Engineering, AU College of Engineering, Andhra University Visakhapatnam for providing necessary support in conducting the experiments.

Appendix A: Experimental Strain Path Equations

Equations obtained by the best fit technique for the experimental strain components of different strain paths were tested by compression.

S No	Condition	Strain path equation
1.	H ₀ /D ₀ =1.0, Cylindrical specimen	$\varepsilon_0 = 1.2977 \varepsilon_z^3 + 2.6093 \varepsilon_z^2 - 0.0617 \varepsilon_z + 0.012$
2.	H ₀ /D ₀ =1.5, Cylindrical specimen	$\varepsilon_0 = 2.6788 \varepsilon_z^3 + 3.0925 \varepsilon_z^2 - 0.1233 \varepsilon_z + 0.063$
3.	H ₀ /D ₀ =1.0, Ring specimen	$\varepsilon_0 = -0.2025 \varepsilon_z^3 + 0.3227 \varepsilon_z^2 - 0.4065 \varepsilon_z - 0.018$
4.	H ₀ /D ₀ =1.5, Ring specimen	$\varepsilon_0 = 3.8586 \varepsilon_z^3 + 3.4659 \varepsilon_z^2 - 0.17 \varepsilon_z + 0.0014$
5.	H ₀ /D ₀ =1.0, Taper specimen	$\varepsilon_0 = -345.69 \varepsilon_z^3 - 57.854 \varepsilon_z^2 - 3.0968 \varepsilon_z - 0.009$
6.	H ₀ /D ₀ =1.5, Taper specimen	$\varepsilon_0 = -1.9953 \varepsilon_z^3 + 0.8844 \varepsilon_z^2 - 0.2144 \varepsilon_z + 0.0014$
7.	H ₀ /D ₀ =1.0, Flange specimen	$\varepsilon_0 = -142.94 \varepsilon_z^3 - 54.875 \varepsilon_z^2 - 8.0465 \varepsilon_z - 0.0059$
8.	H ₀ /D ₀ =1.5, Flange specimen	$\varepsilon_0 = -0.0643 \varepsilon_z^3 - 0.7988 \varepsilon_z^2 - 1.6447 \varepsilon_z + 0.0143$

References

- Altan T, Hannan D, 2002, Forging: prediction and elimination of defects in cold forging using process simulation –The Engineering Research Center for Metal shape manufacturing, <http://www.ercnsm.org>
- Ansys 8.0 reference manual, 2006.
- Brozzo, P., De Luca, B., and Redina, R., 1972, A new method for the prediction of the formability limits in metal sheets, *Proceedings of the 7th Biannual Congress of the International Deep Drawing Research Group (IDDRG), Amsterdam*
- Dieter G.E., 1988 - 3rd edition, Mechanical Metallurgy, McGraw-Hill Book Company-London, pp. 45-46.
- Dieter G.E., 1928 - 1st edition, Mechanical Metallurgy, McGraw-Hill, Book Company London
- Erman E., Kuhn H.A. and Fitzsimons G., 1983, Novel test specimens for workability testing- Compression Testing of Homogeneous Materials and Composites. ASTM STP, Vol. 808, p. 279.
- Gouveia, B.P.P.A., Rodrigues, J.M.C and Martins, P.A.F, 1996, Fracture predicting in bulk metal forming, *Intl. J. Mech. Sci.*, Vol. 38, No 4, p 361-372.
- Hollomon. J. H, 1945, Tensile deformation, *Transactions, AIME*, Vol. 162, p 268-290.
- <http://www.matweb.com>
- Iwahashi Y., Horita Z., Nemoto M., and Langdon T.G., *Factors influencing the equilibrium grain size in equal-channel angular pressing: role of Mg additions to aluminum*, 1998, *Metall. Mater. Trans. A*, Vol. 29, No. 10, pp. 2503–2510.
- Jolgač M, Hamouda A.M.S, Sulaiman.S, Hamdan M. M, 2003, Development of a CAD/CAM system for the closed – die forging process. *J. of Material Processing Technology*, Vol. 138, p 436 – 442.
- Johs A. Bailey – 1969, “The plane strain forging of Aluminum and an aluminum alloy at low strain rates and elevated temperatures, *Intl. J. of Mechanical. Science*. Vol 11, p 491 – 507.
- Kudo, H., and Aoi, K., 1967, *Effect of Compression Test Condition Upon Fracturing of a Medium Carbon Steel – Study on Cold – Forgeability Test*; Part II, *J. of the Jpn. Soc. of Technol. Plast.*, Vol. 8, p 17-27.
- Kobayashi, S., 1970, Deformation characteristics and ductile fracture of 1040 steel in simple upsetting of solid cylinders and rings, *J. of Engineering for Industry, Trans ASME, Series B*, Vol.92, No.2, pp. 391 -399.
- Kobayashi, S, Oh, S.I., and Altan. T., 1989, Metal forming and the finite element method, Oxford University Press, New York,
- Kuhn, H.A., and Lee, P.W., 1971, Strain instability and fracture at the surfaced of upset cylinders, *Metallurgical and Materials Transactions B.*, Vol 2, pp. 3197 – 3202.
- Komura S., Horita Z., Nemoto M., and Langdon T. G., 1999, Influence of stacking fault energy on microstructural development in equal-channel angular pressing, *J. Mater. Res.*, Vol. 14, pp. 4044 – 4050.
- Lee C.H. and Kobayashi S., 1973, New solutions to rigid-plastic deformation problems using a matrix method, *J. Eng.Ind. (Trans. ASME)*, Vol. 95, p. 865.
- Male, A. T., and Cockcroft, M.G., 1964-65, A method for the determination of the coefficient of friction of metals under conditions of bulk plastic deformation, *J. Inst. of Metals*, Vol. 93, p. 38.
- Parteder E, Bunten R., 1998, “Determination of flow curves by means of a compressive test under sticking friction conditions using on iterative finite-element procedure” *J. of materials processing Technology*, Vol. 74, p 227-233.
- Rao J.B., Kamaluddin S, Appa Rao J., Sarcar M.M.M. and, Bhargava N.R.M.R., 2009, Deformation behavior of Al-4Cu-2Mg alloy during cold upset forging, *J. of Alloys and Compounds*, Vol. 471, pp. 128-136.
- Rajiv Shinpuri, 2004, Advances in numerical modeling of manufacturing process: application to steel, aerospace and automotive industries, *Trans. Indian. Inst. Metals*. Vol. 57, No. 4, pp. 345-366.
- Tong W, 1998, Strain characterization of propagative deformation bands, *J. of the Mechanics and Physics of Solids*, Vol. 46, No. 10, pp. 2087 – 2102.
- Thomason, P. F., 1969, Tensile plastic instability and ductile fracture criteria in uniaxial compression tests, *Intl. J. of Mechanical Science*, Vol. 11, p 187-194.
- Ungár T., Gubicza J., Ribárik G., and Borbély A., 2001, Crystallite size distribution and dislocation structure determined by diffraction profile analysis: principles and practical application to cubic and hexagonal crystals, *J. of Applied Crystallography*, Vol. 34, p 298-310.

Vazquez V, Altan T., 2000, New concepts in die design – physical and computer modeling applications, *J. of Materials Processing Technology*, Vol. 98, pp. 212 – 223.

Wu, W.T., Jinn, J.T., and Fischer, C.E., Scientific Forming Technologies Corporation, Chapter 15.

http://www.asminternational.org/Template.cfm?Section=BrowsebyFormat&template=Ecommerce/FileDisplay.cfm&file=06701G_ch.pdf

Zeinkiewicz O.C., 1984, Flow Formulation for Numerical Solution of Forming Processes, in J.F.T. Pittman et al. (Eds), *Numerical Analysis of Forming Processes*, Wiley. New York, pp. 1-44.

Nomenclature

D_b	Bulge diameter	α	Strain ratio (slope of the strain path)
D_e	End diameter	ϵ_z	Axial strain
D_0	Initial diameter of the cylindrical sample	ϵ_θ	Circumferential strain
H_0	Initial height of the cylindrical sample	$\bar{\epsilon}$	Effective strain
H_0/D_0	Aspect ratio	$\bar{\sigma}$	Effective stress
K	Strength coefficient	σ_H	Hydrostatic stress $[(\sigma_r + \sigma_\theta + \sigma_z)/3]$
n	Strain- hardening exponent	σ_r	Radial stress component
R_c	The radius of curvature or radius of circle	σ_z	Axial stress component
w_0	Original width of the square grid	σ_θ	Circumferential stress component
w_i	Current width of the square grid		

Biographical notes

Dr. Babu Rao Jinugu, working as Associate Professor in the Dept. of Metallurgical Engineering, AU College of Engineering, Andhra University, Visakhapatnam since May 2000. He completed his B. Tech and M. Tech in Metallurgical Engineering from NIT Warangal and Ph. D from Andhra University, Visakhapatnam. Prior to join in this University, he worked as Assistant Manager (QA & TD), R&D division of RINL, Visakhapatnam Steel Plant, Visakhapatnam since Sept' 1995-April 2000 and also worked as Scientist in C-MET Laboratories, Dept of Electronics, Hyderabad for a period of two months (August - September 1995). He is the Life member for The Indian Institute of Metals (IIM) – Kolkata, Life Member for Tribology Society of India (TSI) and Life member for The Institution of Engineers (IEI). At present he is holding the positions of Joint Secretary - IIM Visakhapatnam Chapter, Chairman - IIM Visakhapatnam Students Chapter and Member- Editorial Board of IIM News Magazine. Currently working for UGC, New Delhi sponsored Major Research Project (File No: 34 -396/2008 (SR) on “Synthesis and Characterization of Al-Fly Ash Nano Composites” and also working for one AICTE, New Delhi sponsored research project (File No: 1-51/FD/CA/ (19)2006-2007) on “Studies on cold workability limits of Aluminium and its alloys”. He was chosen by AICTE-New Delhi as “Career Award for Young Teacher” in the year 2007. He was visited Beijing, China and Singapore in the year 2008 for participation and presenting the papers at various international conferences. At present, a total of 53 Research Papers were published at various national and International journals/ conferences. His current areas of research are Nano Composite Materials and Metal Forming.

Dr. Syed Kamaluddin, working as Professor & Head of the Department of Mechanical Engg., GITAM University, Visakhapatnam, India. At present, a total of 25 research papers were published at various national and International journals/ conferences. His current areas of research are Metal Forming and finite element analysis.

Dr. NRMR Bhargava, working as Professor in the Dept of Metallurgical Engg, AU College of Engineering, Andhra University, Visakhapatnam, India. He completed his B. Tech in Metallurgical Engineering from NIT Warangal M. Tech from IT BHU, Varanasi and Ph. D from IISc Bangalore. He was visited China and Singapore in the year 2008 for participation and presenting the papers at various international conferences. At present, a total of 85 Research Papers were published at various national and International journals/ conferences. His current areas of research are Composite Materials, foundry and Metal Forming. At present he is working as Registrar, Adikavi Nannyya University, Rajahmundry, AP, India.

Received September 2010

Accepted November 2010

Final acceptance in revised form November 2010